Design and Performance of a Temporary Concrete Diaphragm Wall Excavation Support System in South Boston, Massachusetts

Wystan Carswell, Ph.D., P.E., M.ASCE
Damian R. Siebert, P.E., M.ASCE

Haley & Aldrich, Inc.,
465 Medford Street, Suite 2200,
Boston, MA 02129
wcarswell@haleyaldrich.com
dsiebert@haleyaldrich.com

haleyaldrich.com

Design and Performance of a Temporary Concrete Diaphragm Wall Excavation Support System in South Boston, Massachusetts

Wystan Carswell, Ph.D., P.E., M.ASCE[1] and Damian R. Siebert, P.E., M.ASCE[2]

[1]Haley & Aldrich, Inc., 465 Medford Street, Suite 2200, Boston, MA 02129; e-mail:
wcarswell@haleyaldrich.com
[2]Haley & Aldrich, Inc., 465 Medford Street, Suite 2200, Boston, MA 02129; e-mail:
dsiebert@haleyaldrich.com

Abstract

This paper discusses the design, analysis, and performance of a reinforced concrete diaphragm "slurry" wall temporary excavation support system in South Boston, Massachusetts. The excavation support system was required for construction of two deep below-grade parking garages transected by an existing underground transit tunnel. The excavation was approximately 8.8 m (29 ft) deep for one garage and approximately 14.3 m (47 ft) deep for the other. The excavations were supported with a combination of internal and external bracing. A PLAXIS 2D finite element model using the Mohr-Coulomb constitutive model for soil was used to perform staged construction analyses pre-construction. The model was calibrated post-construction using the Hardening Soil constitutive model based on field measured displacements from inclinometers. The calibrated model indicated that the Hardening Soil model provided better agreement with the actual slurry wall displacements and highlighted the sensitivity of the Boston Blue Clay parameters in the model.

Introduction

This paper is a case study of a unique dual-excavation support project in South Boston, Massachusetts. The project consists of a mixed-use commercial development on a 1.32-hectare (3.27-acre) site transected by the underground Massachusetts Bay Transit Authority (MBTA) Silver Line bus tunnel. The development, EchelonSeaport, includes a two-level retail podium and three high-rise residential towers over two and three levels of below-grade parking covering the entire parcel. Foundation support consists of a mat foundation bearing in the marine clay. Two separate excavations were required for construction of the below-grade parking garages due to the presence of the tunnel through the site. A reinforced concrete diaphragm wall, constructed by the slurry trench excavation method ("slurry wall"), served as both the temporary excavation support system and the permanent foundation wall for the below-grade parking garage and foundation system. The plan area of the garage excavations is shown on Figure 1 and consisted of an approximately 5300 m² (57,000 sq ft) footprint on the north side of the tunnel (Parcel M1) and 3700 m² (40,000 sq ft) on the south side of the tunnel (Parcel M2).

The excavations for the two basement spaces extended to depths of approximately 14.3 m (47 ft) for Parcel M1 (to the north, 2.1 m to 3 m [7 ft to 10 ft] below the bottom of the sloping tunnel) and 8.8 m (29 ft) for Parcel M2 (to the south) below ground surface, (Figure 2; the tunnel ascends from northwest to southeast).
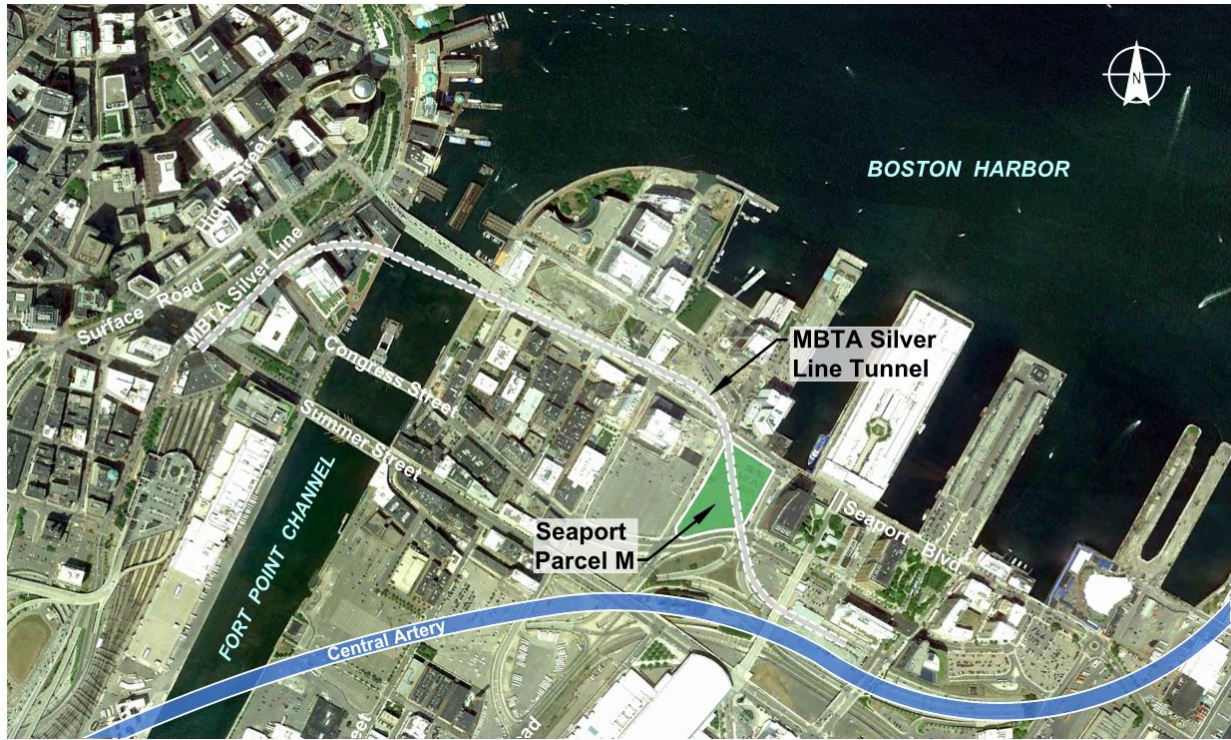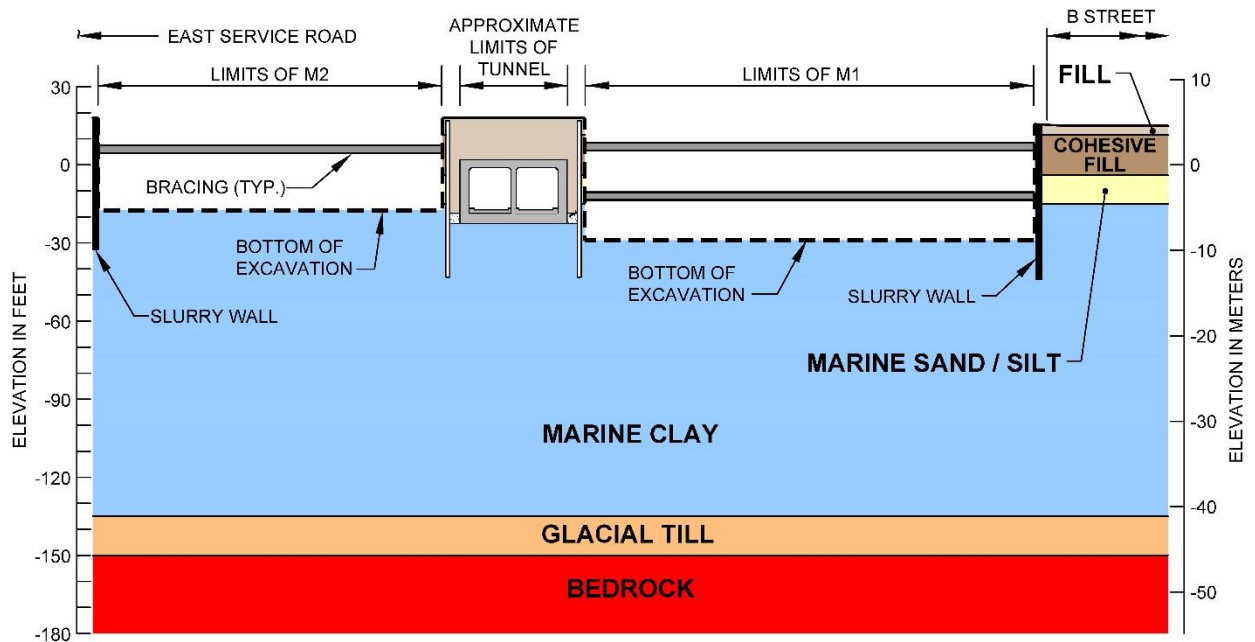
Figure 1. South Boston Seaport Parcel M.

Figure 2. Excavation support system cross-section and subsurface soil profile.

The excavation support system consisted of 0.8 m-thick (30 in.-thick) slurry walls extending typically 4.6 m to 7.6 m (15 ft to 25 ft) below the bottom of the excavation. At specific locations, the slurry wall was designed to support vertical column loads from the above-grade structure by extending the bottom of the slurry wall deeper into the underlying soils to provide adequate vertical foundation capacity through additional frictional/side resistance on the embedded portion of the wall.

The subsurface soil profile is dominated by approximately 30.5 m (100 ft) of marine clay referred to locally as Boston Blue Clay. This deep deposit of clay plays a major role in the design and performance of excavation support systems, as large and deep excavations can lead to deep-seated (global) soil movements. These movements can cause bottom heave within excavations and potentially far-reaching settlement outside the limits of the site. During early phases of development in the South Boston Seaport area there was a higher risk tolerance for ground movements due to excavation, as much of the area consisted of parking lots and had few sensitive structures and utilities; however, by the start of the EchelonSeaport project on Parcel M, there were several newly constructed high-rise structures near the site (in addition to the tunnel running through the site), newly installed public roadways and infrastructure. The project specifications required staged finite element modeling of the excavation to estimate ground movements associated with the project due to the multiple nearby structures and abutters.

The authors acknowledge that a significant amount of coordination, planning, and engineering design was required by multiple parties to make the project a success; however, this paper will focus on a comparison between the ground movements predicted by design and modeling versus measured performance of the excavation support system. Excavation support system performance was assessed by inclinometer data collected on lateral slurry wall deformation and vertical movement of the underground tunnel from survey monitoring points. An overview is provided of the available subsurface information, design methodology, instrumentation and monitoring results, and inverse modeling (i.e., model calibration using measured performance) to assess the design approach and improve estimates of ground movements for future developments.

Elevations are in feet and refer to Boston City Base datum.

Subsurface information

The Seaport area of South Boston, Massachusetts, was a waterfront area of tidal mud flats filled primarily with dredge material during the mid- to late 19th century to create more land for Boston's growing population and industry (Seasholes 2003). The South Boston Seaport transitioned from warehouses and railroads to parking lots in the late 1990s. The subsequent commercial, mixed-use development of the area was spurred by infrastructure investments, most notably for the Central Artery/Ted Williams Tunnel project, leading to the present-day landscape of mid- to high-rise structures. Part of the investment related to infrastructure development included hundreds of test borings along the alignment of the Central Artery tunnel as well as an extensive battery of geotechnical testing to evaluate engineering soil properties (Ladd et al. 1998).

The soil profile of the South Boston Seaport district consists primarily of granular fill underlain by hydraulically placed fill, a thin layer of organics, a deep deposit of marine clay (Boston Blue clay), and very dense glacial till overlying bedrock (Figure 2). The properties and behavior of the hydraulically placed fill varies widely, as the borrow sources and technology for land filling changed over the approximate 30-year period during the incremental filling of the "South Boston Flats." The top of the marine clay typically has a stiff "crust" or over-consolidated zone ranging in thickness between 1.5 m (5 ft) and 4.6 m (15 ft) underlain by a softer zone which is close to normally consolidated.

In addition to the historic soil testing and boring information, Haley & Aldrich performed site-specific geotechnical investigations which included 14 test borings, five cone penetrometer (CPT) tests, and geotechnical laboratory testing including two isotropically consolidated, undrained triaxial compression shear tests of the marine clay.

Temporary support of excavation (SOE) design

The support of excavation (SOE) system was analyzed using a two-dimensional finite element model (PLAXIS 2D), which assumes plane strain conditions. Seven cross-sections were considered for the design, including three sections through the tunnel and two sections each through the north and south excavation (Parcel M1 and Parcel M2 respectively) representing typical internally braced and tied-back sections. This paper focuses on a typical internally braced section in the deeper Parcel M1 excavation (refer to starred location in Figure 3). Detailed discussion of the other sections is outside the scope of this paper.

The design and analysis of the slurry wall was performed using a two-dimensional, plane strain finite element model in PLAXIS 2D with the Mohr-Coulomb constitutive model used for each soil layer (refer to Table 1 for soil properties).

Table 1. Mohr-Coulomb soil properties used for design.

Stratum (Top of Strata Elev.)	Total Unit Weight (kN/m³)	Friction Angle (degrees)	Undrained Shear Strength (kPa)	Modulus, E' (MPa)
Fill	18.9	28	--	3.8
Cohesive Fill	17.3	--	23.9	9.6
Marine Silt and Sand	18.9	32	--	34.5
Marine Clay Crust	18.9	--	83.8	43.1
Lower Marine Clay Deposit	18.9	--	71.8	43.1
Glacial Till	19.6	38	--	86.2
Bedrock	20.4	--	383	268

Figure 3. Excavation support system plan.

The slurry wall was modeled using linear elastic "plate" elements based on Mindlin beam theory, assuming a cracked moment of inertia equivalent to 50% of the gross moment of inertia and a modulus of concrete of 27.8 GPa (580×10^6 psf, for an unconfined compression strength f'_c = 34.5 MPa [5,000 psi]).

As-built drawings were provided for the tunnel, and the elevations shown in the drawings for the top of the tunnel roof were verified by exploratory test pits and probes undertaken by the project design team prior to construction. Similar to the slurry wall modeling above, the tunnel was modeled using plate elements assuming an effective moment of inertia (I_e) equivalent to 50% of the gross moment of inertia (to take into account the effects of surficial cracking) and a modulus of concrete of 24.8 GPa (519×10^6 psf, for an unconfined compression strength of f'_c = 27.6 MPa [4,000 psi]). Interface elements were used between the structural plate elements and the soil, and the interface strength reduction factor (R_{inter}) was assumed to be 0.67.

Internal bracing was modeled as fixed-end anchors in PLAXIS. The braces were assumed to be spaced 7.6 m (25 ft) on center with a uniaxial stiffness corresponding to 91.4 cm (36-in.) diameter pipe struts with 1.3 cm (0.5 in.) wall thickness and a length of 15.2 m (50 ft). While typically internal bracing is preloaded to 50% of the design axial load after installation, the bracing installed against the tunnel were preloaded to approximately 25% of the design load (1.1 MN [250 kips] in the model) to minimize possible impacts to the tunnel due to brace preload jacking.

During different phases of construction, either a 9.1-m-wide (30 ft-wide) surface construction surcharge of 11.5 kPa (240 psf) (centered over the top of the tunnel) or a 9.1-m-wide (30-ft-wide) surface construction surcharge of 28.7 kPa (600 psf, set back 1.5 m [5 ft] from the slurry wall) was assumed behind the slurry wall sections.

The model predicted maximum lateral slurry wall deformations in the range of 36 mm to 69 mm (1.4 in. to 2.7 in.), less than the 89 mm (3.5 in.) limiting performance criteria established in the project specifications.

Predicted maximum downward movement of the tunnel was 28 mm to 56 mm (1.1 in. to 2.2 in.). The tunnel was analyzed by the project structural engineer for the shear, moment, and deformation of the tunnel from the model output and was deemed to have adequate capacity for the loading conditions imposed by construction.

Temporary support of excavation system performance

An instrumentation and monitoring program was established to monitor performance of the SOE system during excavation, which included twelve (12) inclinometers extending to glacial till, four (4) observation wells outside the excavation limits, five (5) tunnel monitoring points, and over 100 other survey reference points for monitoring movement of utilities, street surfaces, and adjacent structures. In addition to quantitative monitoring, a camera stationed on a building across Seaport Boulevard recorded photographs of the site from a high vantage point approximately every 15 minutes, allowing for a transparent assessment of construction activities on the site. The inclinometers were read approximately every two to four weeks after initialization, depending on the stage of excavation and access to the inclinometer locations.

Soil mixing was performed along the slurry wall alignments adjacent to the tunnel to stabilize the fill soils prior to slurry wall construction. The soil mix had a target strength of 345 kPa to 483 kPa (50 psi to 70 psi) and was conducted to approximately 12.2 m (40 ft) below ground surface and for a width of approximately 3 m (10 ft) centered on the slurry wall alignment. While not part of the original scope of the project, the soil mixing was proposed by the contractor due to their experience with slurry wall panel excavation collapse in granular backfill adjacent to the tunnel on an adjacent parcel. This additional protective measure was successful as no panel collapses or significant concrete overpours occurred in this zone during slurry wall installation.

Most of the lateral slurry wall movement (as measured by the inclinometers) occurred during the final excavation stage, prior to pouring the mat foundation, but the maximum lateral slurry wall movement for Parcel M1 occurred after the removal of the second level of bracing. The maximum theoretical lateral deformation of the slurry wall compared to the measured maximum deformation is shown in Table 2, where in all cases the maximum deformation occurred 6.1 m to 9.1 m (20 ft to 30 ft) below the top of the slurry wall inward toward the excavation.

Table 2. Theoretical vs. measured maximum lateral deformation of the slurry wall.

Parcel/Excavation	M1/North		M2/South	
Section	Max. Theoretical Deformation (mm)	Max. Measured Deformation (mm)	Max. Theoretical Deformation (mm)	Max. Measured Deformation (mm)
Typical Tieback	58	69	51	43
Typical Internally-Braced*	58	23	66	23
Center Cross-Section of Tunnel	58	94	56	33

*Section used for model calibration.

Generally, the measured lateral deformation of the slurry wall for Parcel M1 was larger than predicted and the lateral deformation of the slurry wall for Parcel M2 slurry wall was smaller than predicted. Estimation of lateral deformation for the tieback sections were within approximately 10-15% of the measured values, while the measured lateral deformation for the typical internally braced sections were approximately 35-40% of the predicted. The estimations of maximum lateral deformation for the center cross-section of the tunnel diverged: The slurry wall deformation north of the tunnel (Parcel M1) was approximately 60% more than theoretical, and the slurry wall deformation south of the tunnel (Parcel M2) was approximately 65% less than theoretical. These departures are likely due to a combination of soil and structure modeling assumptions and the complicated soil stress history in this location (prior structures with wood pile foundations, construction of the tunnel, and soil mixing prior to excavation).

Despite the lateral slurry wall deformation measured by the inclinometers, survey measurements of the tunnel indicated minimal vertical movement – approximately an order of magnitude smaller than what was estimated by the Mohr-Coulomb model: The maximum measured settlement was approximately 6.4 mm (0.25 in.) near the center cross-section of the tunnel, and approximately 6.6 mm (0.26 in.) of upward vertical movement (heave) was recorded near the southern portion of the tunnel.

Inverse modeling

Inverse modeling (i.e., model calibration) was performed in PLAXIS 2D using the measured lateral slurry wall deformation from inclinometers to better capture the ground movements associated with the excavation and to better understand the in-situ soil properties. The inverse modeling focused on a typical braced section on the eastern wall of Parcel M1 (starred location in Figure 3), as the three-dimensional effects (e.g., stiffening near the corners of the excavation) were less pronounced in this section, and therefore the two-dimensional plane strain finite element model was more able to capture the measured behavior. Additionally, the relative simplicity of the model allows for a more focused study of the soil-structure interaction of the SOE system during excavation.

Several factors were considered in the model calibration, including:

Groundwater. Groundwater readings from observation wells near the excavation indicated that the design groundwater level (approximately 2.1 m [7 ft] below ground surface) was an appropriate assumption for the model.

Construction surcharge. A review of the construction camera footage indicated that little to no vertical construction surcharge was sustained at the location of the inclinometer location in question; construction surcharge was therefore removed from the finite element model.

Slurry wall and bracing. The calibrated model used two-dimensional finite elements to model the slurry wall with a linear elastic, perfectly plastic constitutive model. Concrete cylinder breaks of the slurry wall concrete mix design had an average unconfined compressive strength of f'_c = 54.5 MPa (7910 psi); the linear elastic modulus of the slurry wall concrete material was increased to 35GPa (730×10^6 psf) to correspond to this compressive strength. Slurry wall installation was also simulated prior to the excavation stages by modeling an excavated trench with equivalent fluid pressure of 11.3 kN/m^3 (72 pcf) to represent the slurry (i.e., triangular load distribution on side walls and uniform pressure on the bottom of the panel excavation). The bracing stiffness was refined to reflect the internal bracing at that location, averaging the stiffness, length, and spacing of the braces installed. The stiffness of the upper level of bracing decreased by approximately 30% as compared to the original design and was increased by approximately 20% for the lower level of bracing.

Soil profile. The soil profile modeled was adjusted from the generalized section used for internal bracing in Parcel M1 to match the strata defined by the nearest boring and CPT investigation: Most significantly, the thickness of the marine sand and silt layer was increased from 3.4 m to 5.8 m (from 11 ft to 19 ft), and the strata break between the marine sand and silt to marine clay was lowered by 2.1 m (7 ft). From the special testing performed by Ladd et al. (1998) in South Boston, the bottom of the clay crust in South Boston was defined as approximately El. -16.5 m (El. -54 ft); this is supported by the soil descriptions in the nearest boring log (historic, recorded by others) which describe a transition from stiff, silty clay to medium stiff clay approximately 4.6 m (15 ft) deeper than where the bottom of the marine clay crust was modeled. The clay crust layer was extended to El. 13.7 m (El. -45) in the calibrated model.

Strength properties. A cone factor (N_{kt}) of 12 was used to convert the site-specific CPT data (Figure 4) to undrained shear strength based on the work of Ladd and DeGroot (2003) on Boston Blue Clay from South Boston Central Artery/Tunnel testing. Based on this data conversion, the undrained shear strength profile of the marine clay was increased to follow the approximate average of the CPT data and above the results from the two isotropically consolidated, undrained compression (CIUC) triaxial tests (Figure 4; it could also be noted that the soil samples used for the two triaxial tests had a Sample Quality Designations in the range of C to D based on the volumetric strain at in situ stress, per Terzaghi et al., 1996).

For the marine sand and silt layer, a review of the standard penetration test blow counts from the nearest boring indicated that an average *N*-value of 28 was representative of the stratum corresponding to a friction angle of 34 degrees (vs. the 32 degrees used in the initial design) when using the empirical correlations of Duncan and Buchigani (1976). According to the CPT data using the Kulhawy and Mayne (1990) method, the friction angle could have been increased to as much as 40 degrees. Given the description of the sand as medium dense to dense, a friction angle of 34 degrees was selected for the calibrated model.
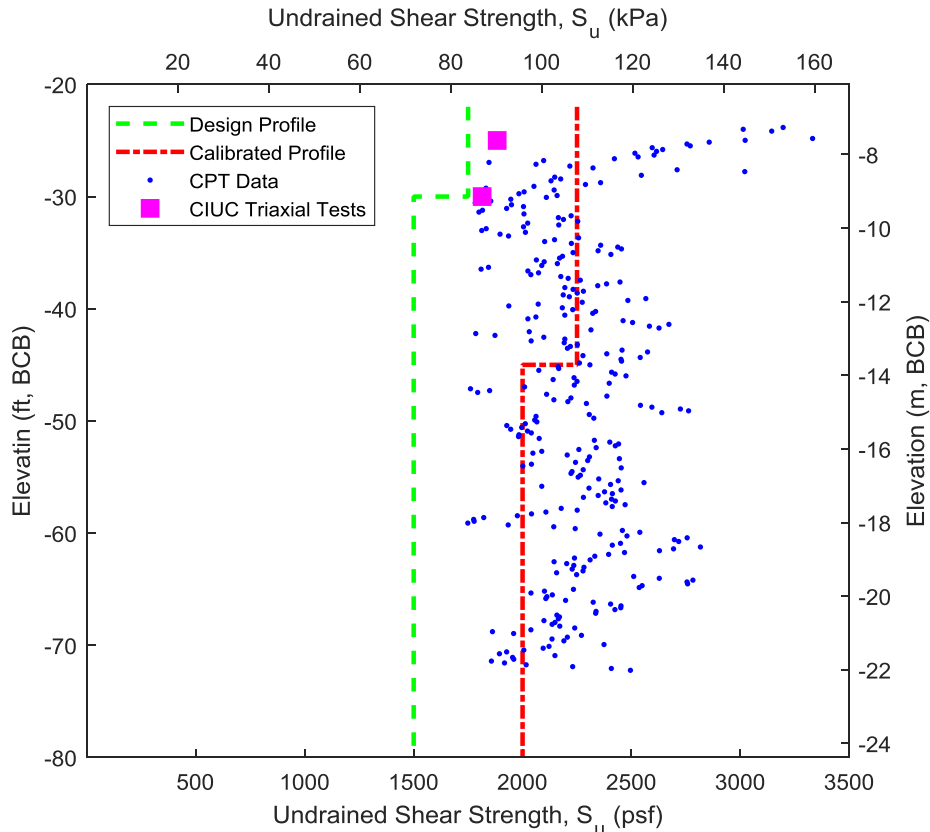
Figure 4. CPT Data (using N_{kt} = 12) and isotropically consolidated undrained compression triaxial (CIUC) test results with undrained shear strength (S_u) profiles.

Constitutive models and stiffness parameters. To account for stress-dependent stiffness, the marine sand and silt and marine clay crust were modeled using the Hardening Soil (HS) constitutive model, and the lower marine clay deposit was modeled using the Hardening Soil with Small Strain (HSS) constitutive model. The fill, cohesive fill, glacial till, and bedrock strata were modeled using the same Mohr-Coulomb constitutive model and properties as before; as there was little new information acquired for these strata, and the influence on the model results was minimal due to the location of the strata and the proportion of the soil profile.

In addition to the input parameters used for Mohr-Coulomb models, the HS and HSS models require definition of the secant modulus at 50% of the maximum stress (E_{50}, typically ascertained from triaxial testing), a tangent oedemetric modulus (E_{oed}), and an unload-reload modulus (E_{ur}). These moduli are selected for a minor principal reference stress (p_{ref}, typically taken as 100 kPa [2089 psf]) and then vary based on the confining stress of the soil element (taken here to be a function of the in-situ vertical effective stress, σ'_{v0}) and account for stress-level dependency through the power coefficient m.

The model was calibrated considering three construction stages: excavation for the installation of the second level of bracing, excavation to install the mat foundation (bottom of excavation), and the removal of the second level of bracing after the mat foundation was poured (refer to Figure 2). Selection of stiffness properties of in the constitutive models were subject to the following criteria:

- For the marine sand and silt layer, E_{50} was bounded by $150\sqrt{K_0\sigma'_{v0}/p_{ref}}$ and $600\sqrt{K_0\sigma'_{v0}/p_{ref}}$ based on the testing and observations from Janbu (1963), where K_0 is the at-rest earth pressure coefficient and E_{oed} was assumed to be $1.5E_{50}$ (Schanz and Vermeer, 1998).
- For the marine clay crust, E_{50} was bounded by $100\sigma'_{v0}$ and $700\sigma'_{v0}$ (Ladd et al., 1998), E_{oed} was assumed to be equal to E_{50} and E_{ur} was limited to $10E_{50}$.
- For the lower marine clay deposits, E_{50} was bounded by $100\sigma'_{v0}$ and $400\sigma'_{v0}$ for the marine clay (Ladd et al., 1998), E_{oed} was assumed to be equal to E_{50}, and E_{ur} was limited to $10E_{50}$.
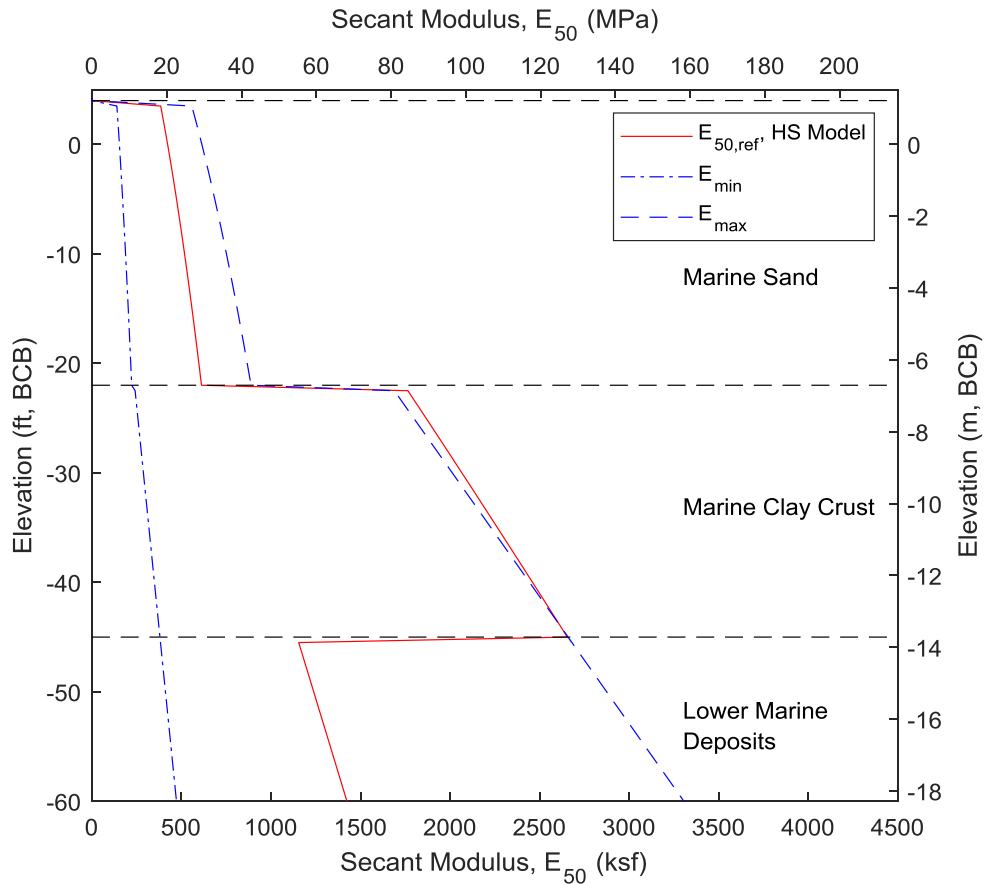

Figure 5. Calibrated E_{50} secant modulus for marine sand and silt, marine clay crust and lower marine deposits relatively to minimum and maximum bounds

The model was calibrated by iteratively adjusting soil parameters within the bounds listed above to best match the deformed slurry wall shapes measured by the inclinometer at the three selected construction stages. An approximately average value of E_{50} was selected for the marine sand and silt layer and a slightly above-average value was selected for the lower marine deposits (where "average" is in reference to the previously defined minimum and maximum bounds, Figure 5). The approximate maximum bound was selected for the marine clay crust stratum.

Table 3 shows the resulting HS properties that were used in the calibrated model with associated wall deformations shown in Figure 6.

Table 3. Hardening soil properties estimated by inverse modeling.

Stratum	Total Unit Weight (kN/m³)	Friction Angle (degrees)	Undrained Shear Strength (kPa)	E_{50} (MPa)	E_{oed} (MPa)	E_{ur} (MPa)	m
Marine Silt and Sand	18.7	34	--	57.5	86.2	287	0.5
Marine Clay Crust	19.5	--	108	74.2	74.2	383	0.9
Lower Marine Clay Deposit*	19.5	--	95.8	30.2	30.2	302	1

*The lower marine clay used an HSS model with shear modulus G_0 = 120 MPa (2500 ksf) associated with shear strain at 70% of the maximum shear modulus, γ_0 = 1.5 × 10⁻⁴.
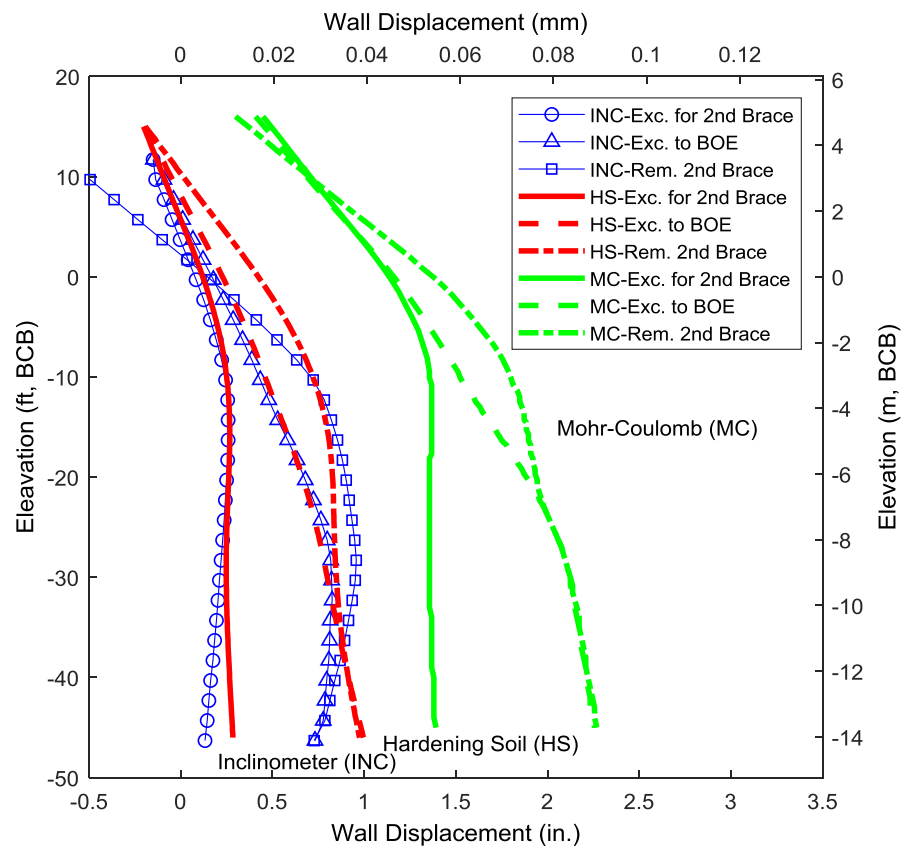

Figure 6. Theoretical predictions of lateral slurry wall movement compared to inclinometer data.

Discussion

The calibrated model using the HS and HSS soil models was able to capture the performance and deformation of the wall much more accurately than the original Mohr-Coulomb model. Slurry wall performance was predominantly controlled by the properties of the marine clay crust and lower marine clay deposit, where the unload-reload modulus E_{ur} controlled lateral wall movement during early stages

of excavation (i.e., the excavation to for the second level of bracing), and the secant modulus E_{50} controlled toe movement (i.e., movement at the bottom of the slurry wall) in the later excavation stages.

The strength parameters for the marine sand and silt layers had a minor influence on slurry wall deformation and shape, but an adjustment of the unit weight to 18.7 kN/m^3 (119 pcf) improved the performance of the PLAXIS model relative to the inclinometer readings.

The use of higher-order constitutive models (HS or HSS) for the fill, cohesive fill, glacial till, and bedrock strata had no significant influence on the performance of the wall, nor did the manipulation of soil properties in these strata lead to significant changes in slurry wall deformation shape.

The calibrated model's inability to fully capture the behavior of the slurry wall near the toe of the wall may imply that the clay strata are stiffer than expected; however, while increasing the unload-reload modulus E_{ur} for the marine clay would have the most immediate impact on the modified PLAXIS model results, the stiffness of the marine clay crust and lower marine deposits were calibrated to be at the maximum range defined at the onset by empirical relationships found in literature. Consequently, while increase of E_{ur} would have resulted in a better "matched" response, the properties selected would not be particularly realistic.

From a design perspective, the most important output of a model is a combination of both the maximum deflection (to meet performance requirements set out in project specifications) and the internal loads for the SOE wall (moment and shear). In order to compare the theoretical loads from the models to field conditions, the moment in the slurry wall M was back-calculated from the inclinometer data deflection data using the second derivative of displacement in which $M = E_c I_e \dfrac{d^2 u}{dy^2}$ where u is the lateral deflection (displacement) from the inclinometer at elevation y, E_c is the modulus of the slurry wall, and I_e is the effective moment of inertia of the slurry wall (assumed to be 50% of the gross moment of inertia of the slurry wall). Because the inclinometer readings were performed every 61 cm (2 ft) and the changes in slope were relative small, the back-calculated moment by derivation is a coarse estimate of the slurry wall moment (Figure 7). A comparison of the back-calculated moment, design moment envelope (from the original Mohr-Coulomb model), and the calibrated model results after the removal of the second level of bracing is presented in Figure 7.
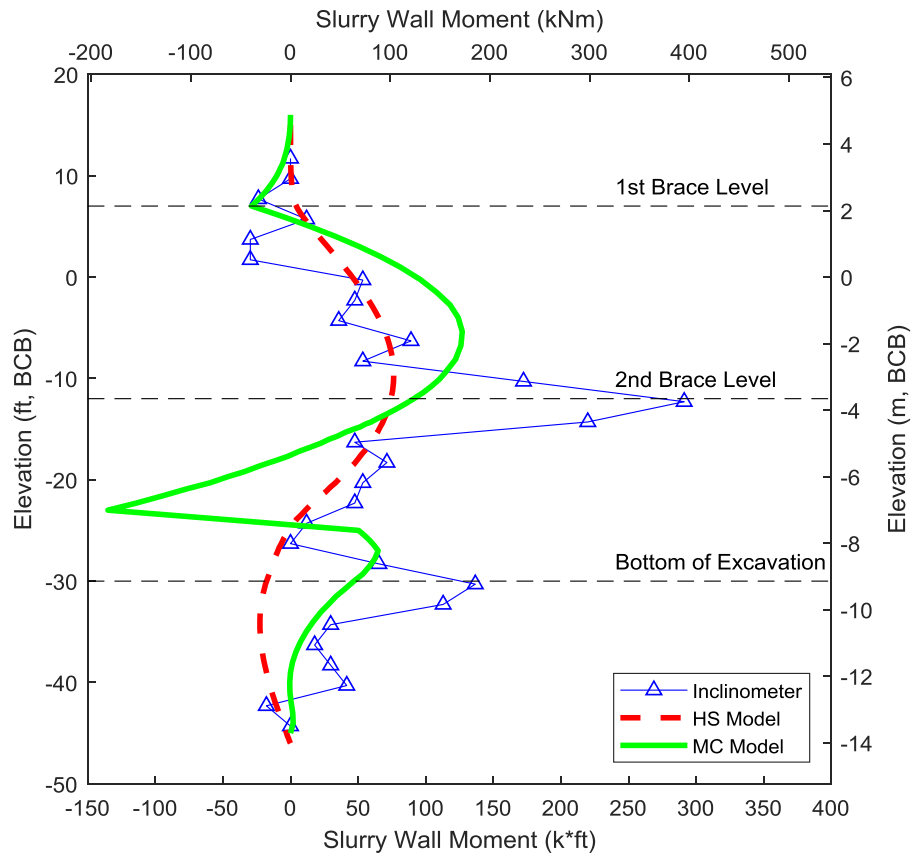
Figure 7. Back-calculated and theoretical moment in the M1 slurry wall

after the removal of the second level of bracing, where positive moment corresponds to tension on the excavation face of the wall and compression on the soil face of the wall.

The calibrated model did not capture the magnitude of the moment at the second brace level nor at the bottom of excavation. The stiffness of the slurry wall in the calibrated model may have been too stiff to form the curvature (and therefore to achieve the inflection points and "peaks" in moment) exhibited by the back-calculated data and the Mohr-Coulomb model. Consequently, while the wall deformation shapes in Figure 6 appear relatively consistent with the observed data (perhaps implying a reasonably good calibration of the soil materials in the model), the calibrated model's moment output at this stage of construction considerably underestimated the moment demand.

Despite the Mohr-Coulomb model's inaccurate predictions of slurry wall deformation for the typical internally braced section (Table 2), the moment output from the Mohr-Coulomb model shows several of the inflection points of the back-calculated moment (e.g. the peaks in positive moment between the second brace level and at the bottom of excavation); this implies that the deformation of the wall predicted by the Mohr-Coulomb model was reasonably accurate, and that the discrepancy between maximum observed lateral deformation and predicted is due to the large lateral translation (rigid body movement) of the bottom of the slurry wall in the model (as seen in Figure 6).

Because no cracking was observed in the panels at this location of the slurry wall, the magnitude and precise locations of the peaks in back-calculated moment may be due in part to the lack of data resolution and precision in inclinometer readings; additionally, it should be noted that the back-calculated moment varies linearly as a function of the wall stiffness ($E_c I_e$), when the effective moment of

inertia I_e actually varies along the height of the wall as a function of moment (Nawy, 2009). For instance, the gross moment of inertia I_g would be appropriate to use for sections of the wall which are below the cracking moment ($f_r I_g / y_t$, where f_r is the modulus of rupture and y_t is the distance from the neutral axis to the extreme fiber of the section – half the depth of a rectangular section, e.g.), but a value smaller than I_g would be more appropriate the central portion of the wall where the moment demand is higher.

Conclusions

The performance of two excavations (transected by the tunnel) supported by braced, reinforced concrete diaphragm "slurry" wall support of excavation (SOE) systems in South Boston, Massachusetts, was measured using a combination of survey monitoring points and inclinometers. The inclinometer data was used to inverse model (i.e., calibrate) the performance of a typical internally-braced section of the slurry wall in Parcel M1 (the northern excavation) using a two-dimensional PLAXIS finite element model to better understand the interaction between the slurry wall and the soil during the excavation process for future excavation support design.

Conclusions of this study can be summarized as follows:

- The original Mohr-Coulomb PLAXIS models did not accurately capture slurry wall deformations for internally braced sections. The wall deformations for sections of the wall supported by external tiebacks were reasonably accurate (within 10-15%), deformation for typical internally braced sections were overpredicted (by approximately 35-40%), and the model cross-sections showed diverging estimations (underpredicted for the Parcel M1 slurry wall to the north by 60% and overpredicted by 65% for the Parcel M2 slurry wall to the south). Vertical deformation of the tunnel was significantly overpredicted (by an order of magnitude).
- Inverse modeling of a typical internally braced slurry wall section using the Hardening Soil (HS) and Hardening Soil with Small Strain (HSS) constitutive models in PLAXIS 2D was able to capture the deformation behavior of the wall with reasonable success once differences in construction surcharge, slurry wall stiffness, soil profile, and soil strength characteristics were accounted for. Changes in stiffness for the marine clay layer near the bottom of excavation to the bottom of slurry wall had the most significant impact on slurry wall deformation.
- The inclinometer data was used to back-calculate an estimate of the moment in the slurry wall. While the calibrated model provided a reasonable visible match with the deformation behavior of the slurry wall, the stiffness of the modeled wall was not able to capture the curvature measured by the inclinometer data and therefore "damped" out peaks in the back-calculated moment. Both the original Mohr-Coulomb model and the calibrated HS/HSS model underpredicted the peak moment estimated from the back-calculated inclinometer data, though the coarseness of the inclinometer data may play a role in the magnitude and location of the back-calculated moment peaks. The Mohr-Coulomb model captured some moment inflections in the back-calculated moment curve, implying that rigid body movements in the model (translation at the bottom of the slurry wall) may be the primary cause of inaccuracy in maximum lateral slurry wall deformation estimates.

While preliminary slurry wall design may be performed using a Mohr-Coulomb model, theoretical estimates of slurry wall deflection may benefit from using HS/HSS constitutive models for finalizing design. Because the stiffness parameters of the soil strata near the bottom of the wall had the most significant influence on lateral slurry wall deformation, future designs should consider lab testing

which measures the stress-strain properties of the soil (e.g., triaxial testing) at several depths in this region for interpretation of stiffness parameters.

Pre- and post-cracking stiffness were not considered in this study; further investigation of the nonlinearity in the slurry wall modeling may improve the ability of the model to capture the wall deformation witnessed after the removal of the second level of bracing.

Inverse modeling by optimization of a performance function through an iterative, automated process would improve the model calibration, as well as the inclusion of nonlinear stiffness for the slurry wall.

Future excavations could consider using survey monitoring points at inclinometer locations to supplement and enhance the slurry wall deformation data resolution, increasing the number of points and thereby possibly reducing the noise seen in the back-calculated moment curve in this paper (Figure 7). Additionally, strain gauges on the slurry wall reinforcement could be used as a point of comparison and calibration for the back-calculated moment results.

References

Duncan, J.M. and Buchignani, A.L. (1976). *Geotechnical Engineering: An Engineering Manual for Settlement Studies*. Department of Civil Engineering, University of California – Berkeley.

Kulhawy, F.H. and Mayne, P.W. (1990). *Manual on Estimating Soil Properties for Foundation Design.* Electric Power Research Institute (EPRI) Report EL-6800.

Janbu, N. (1963). "Soil Compressibility as Determined by Oedometer and Triaxial Tests." *European Conference on Soil Mechanics and Foundation Engineering*. Wiesbaden, Germany, Vol. 1, pp. 19-25.

Ladd, C.C. and DeGroot, D.J. (2003). "Recommended Practice for Soft Ground Site Characterization: Arthur Casagrande Lecture." *12th Panamerican Conference on Soil Mechanics and Geotechnical Engineering*. Massachusetts Institute of Technology, Cambridge, MA, 22-25 June 2003.

Ladd, C.C., Young, G.A., Kraemer, S.R., and Burke, D.M. "Engineering Properties of Boston Blue Clay from Special Testing Program." *Special Geotechnical Testing, Central Artery/Tunnel Project in Boston, Massachusetts*, ASCE Special Publication No. 91. J.R. Lambrechts ed. Boston, Massachusetts, 18-21 October 1998.

Nawy, E.G. (2009). *Reinforced Concrete: A Fundamental Approach.* 6th ed.

Schanz, T. and Vermeer, P.A. (1998). "On the Stiffness of Sands." *Pre-Failure Deformation Behavior of Geomaterials*, pp. 383-387.

Seasholes, N.S. *Gaining Ground: A History of Landmaking in Boston.* MIT Press. Cambridge, Massachusetts.

Terzaghi, K., Peck, R.B. and Mesri G. (1996). *Soil Mechanics in Engineering Practice.* John Wiley and Sons, New York.